Zeff Measurement and Analysis of Reheat-Mode Discharges in W7-AS

S. Morita*, J. Baldzuhn
Max-Planck-Institut für Plasmaphysik, D-85748 Garching, Germany
* on leave from National Institute for Fusion Science, Nagoya 464-01, Japan

IPP III / 199 November 1994

MAX-PLANCK-INSTITUT FÜR PLASMAPHYSIK

85748 GARCHING BEI MÜNCHEN

MAX-PLANCK-INSTITUT FÜR PLASMAPHYSIK

GARCHING BEI MÜNCHEN

Zeff Measurement and Analysis of Reheat-Mode Discharges in W7-AS

S. Morita*, J. Baldzuhn

Max-Planck-Institut für Plasmaphysik, D-85748 Garching, Germany

* on leave from National Institute for Fusion Science, Nagoya 464-01, Japan

IPP III / 199 November 1994

Die nachstehende Arbeit wurde im Rahmen des Vertrages zwischen dem Max-Planck-Institut für Plasmaphysik und der Europäischen Atomgemeinschaft über die Zusammenarbeit auf dem Gebiete der Plasmaphysik durchgeführt.

ABSTRACT

The effective charge Z_{eff}, taken as a line-averaged signal in the W7-AS stellarator, is measured for ECH and NBI plasmas by using bremsstrahlung in the visible region at a wavelength of 5202 Å. Any disturbing offset on the bremsstrahlung signal can be avoided in our measurements because any contribution of line radiation from metallic impurities is negligible in the wavelength interval chosen. As a consequence, the Z_{eff} value is successfully obtained even in the low-density region ($< 2 \times 10^{13} cm^{-3}$) of ECH plasmas. Typical values measured for Z_{eff} range from 1 to 2 for NBI plasmas and from 1 to 3 for ECH plasmas in the case of a freshly boronized vessel wall. In some cases of counter-injected NBI, however, larger Z_{eff} values of 3 to 6 are measured. This behavior is similar to that observed in CHS. The results of Z_{eff} measurements on ATF and CHS heliotron/torsatron, on the one hand, and the W7-AS advanced stellarator, on the other, are compared. Clear differences between the devices mentioned are found which originate in the fact that titanium gettering is performed in ATF and CHS, whereas in W7-AS the vessel wall is boronized. We observe a reduction of the Z_{eff} values for the W7-AS plasmas in comparison with those of other machines. This analysis is also done for investigating the impurity behaviour of reheat-mode discharges in W7-AS. During the reheat mode a correlation between the temporal behavior of τ_p and τ_E can be observed, both in W7-AS and CHS.

1. INTRODUCTION

In helical systems the electron density profiles exhibit a specific behavior, depending on the auxiliary heating chosen with either ECH or NBI [1,2]. Especially, the density profile shape may frequently become flat or even hollow. This suggests a low inward velocity of incoming particles in the outer region of the plasma. This flat density profile leads to enhancement of radiation losses and a temperature decrease in the vicinity of the plasma edge. Additionally, the connection length of field lines in the helical device is believed to be shorter than in tokamaks [3]. This might be one of the other reasons why the edge plasma temperature is relatively low in helical devices.

Extensive experimental effort has been made to control the edge plasma. In W7-AS, boronization is extensively carried out, mainly to reduce metallic impurities. It is a limiter experiment with two boronized graphite limiters (20% B, 80% C) to make a clearly defined source for the particle influx and reduce the heat flux to the vacuum wall [4]. In ATF and CHS titanium gettering is carried out to suppress hydrogen and oxygen influx [5].

It is necessary for helical devices to determine the optimum wall treatment. In particular, it is important to study and improve the behavior of the edge plasma in helical devices. Therefore, different machines have to be compared in respect of impurity behavior.

Z_{eff} measurement using visible bremsstrahlung is one of the most appropriate means for this purpose [6,7]. The Z_{eff} value is a typical measure of the impurity behaviour and it is very convenient for analyses covering several plasma shots. Additionally, the visible system for the measurement can be absolutely calibrated by using a standard lamp. The performance is also useful for comparing different plasma devices.

In this report, results of a comparison of Z_{eff} measurements in typical discharges of W7-AS, ATF and CHS are described. The same analytical method is applied for all machines. Especially, in W7-AS

and CHS the same instrument is used to detect the visible bremsstrahlung.

W7-AS is an advanced stellarator (R=2m, <a>=14-17.5cm, B_t=2.5T) with a modular coil system. Therefore, the magnetic surface structure near the last closed flux surface (LCFS) takes a different form to an heliotron/torsatron like ATF and CHS, which have a continuous helical coil system. The rotational transform in W7-AS is almost constant for different minor radii. The ATF and CHS heliotron/torsatrons, however, have a positive shear for normal operation.

Recently, an increase in stored energy (W_p), impurity accumulation and electron density profile peaking had been observed in CHS NBI discharges when the gas puff rate was rapidly reduced (reheat-mode) [8]. The reduction of the neutral density in the peripheral plasma region leads to an increase in both the edge electron and ion temperatures and enhances the edge rotation velocity, whereas the energy losses due to the neutrals through charge exchange and excitation/ionization become less dominant in the outer region of the plasma. At present the origin of the reheat-mode is not clear. However, study of the reheat-mode for different types of helical systems is important for a better understanding of the role of neutral hydrogen near the plasma edge. In CHS the reheat mode does not occur in the case of completely limiter-dominated plasmas, whereas the onset of MHD activity is observed because of the increased pressure gradient. Furthermore, the reheat-mode does not appear in ECH plasmas. This probably originates in the low operational region (53GHz) of the electron density in the ECH plasmas of CHS. In W7-AS however, experiments on the reheat-mode can easily be carried out by using limiters, and the machine allows higher densities even with ECH at 70 and 140 GHz.

2. EXPERIMENTAL SETUP

The system for the visible bremsstrahlung measurement consists of a lens, an optical fiber, an interference filter and a

photomultiplier. The lens determines a certain solid angle for detection of the line-integrated bremsstrahlung. Two lenses are prepared for the measurement. One is small with a diameter of 7mm (focusing length; f=10mm) and the other one is large with a diameter of 16mm (f=20mm). They give viewing areas of 8.2cmϕ and 4.8cmϕ respectively, at a distance of 1m from the lenses. The small lens is normally used for this measurement because it is very convenient to install within the limited space of a diagnostic port.

The optical fiber has a diameter of 0.8mm for the effective transparent area and a length of 25m from the diagnostic port to the photomultiplier. It is an UV-grade fiber with transmission rate close to 100% in the visible range. A photomultiplier of the Hamamatsu R453 type (head-on type) with a diameter of 28mmϕ is used because its sensitivity is stable even for stray magnetic fields below 3G. For the experiments the photomultipliers are placed in the control room.

The wavelength range for detecting the bremsstrahlung continuum is carefully examined in CHS, where the main impurities are carbon, oxygen and titanium, and wavelengths of 5202Å ($\Delta\lambda_{FWHM}$=30Å) and 5377Å ($\Delta\lambda_{FWHM}$=19Å) are finally selected.

In W7-AS, boronization is carried out and B-C limiters are used. Therefore, the main differences concerning impurities are governed by these boronizations. Since the line radiation in W7-AS was not examined in detail, the bremsstrahlung signals are measured with both filters (typical example; #25199-#25235 for 5377Å and #25236-#25242 for 5202Å). As a result similar time behaviors for the two filters are obtained. Besides, the signals also show the same time behavior as an already installed W7-AS bremsstrahlung signal, which usually operates at a wavelength of 5550Å. We normally used the signal from the detector with the filter of λ_o=5202Å because the bandwidth of the filter is wide and a higher intensity can be expected. The transmission curve of the 5202Å filter is shown in Fig.1. The peak transmission rate is 73% at a wavelength of 5202Å. The band width at the wing of the transmission curve is roughly 200Å with a transmission rate of less than 1.5%. The system is absolutely calibrated by an NBS standard tungsten lamp.

The two sets of fibers are installed at port M3-5' (toroidal angle $\phi = -10.2°$) near a toroidal coil for the purpose of visible bremsstrahlung and Hα measurements, as shown in Fig.2. This is a reliable toroidal location for the bremsstrahlung measurement because that position is far from toroidal positions where NBIs for heating, limiters, ICRF antenna are located or where gas puff is carried out. The cross-sectional view at the poloidal location of M3-5' is shown in Fig.3. The angle of detection is set horizontal (poloidal angle $\theta = 0°$). The viewing angle for the measurement is indicated by a hatched area. The distance from the lens to the plasma center is 0.8m. This corresponds to a viewing area of 6cmϕ at the plasma center. No special treatment is applied to the vacuum wall at the opposite side of the viewing angle.

3. CALCULATION OF Z_{eff}

The bremsstrahlung (free-free) radiant flux in a plasma with a Maxwellian velocity distribution is given by [9]

$$\frac{\Delta P_{ff}}{\Delta\lambda} = \frac{16e^6}{3c^2}\left(\frac{\pi}{6m_e^3}\right)^{1/2} \frac{n_e n_i Z_i^2 \bar{g}_{ff}}{T_e^{1/2}\lambda^2} \exp\left(-\frac{hc}{T_e\lambda}\right) \qquad (1)$$

where n_i is the ion density for the charge state Z_i and $\bar{g}_{ff}$ is a temperature-averaged free-free Gaunt factor. A free-bound recombination continuum does not exist in the visible wavelength range. Since magnetically confined plasmas generally include many kinds of impurities with various charge states, formula (1) can be rewritten as

$$\varepsilon_\lambda = \frac{\Delta P_{ff}}{\Delta\lambda} = \frac{1.89\times10^{-28} n_e \sum_i n_i Z_i^2 \bar{g}_{ff}}{T_e^{1/2}\lambda^2} \exp\left(-\frac{12400}{T_e\lambda}\right) \quad [W\cdot cm^{-3}\cdot Å^{-1}] \qquad (2)$$

where n_e, n_i, T_e and λ are given in units of cm^{-3}, cm^{-3}, eV and Å, respectively. The effective charge Z_{eff} is defined by

$$Z_{eff} = \sum_i n_i Z_i^2 / \sum_i n_i Z_i = \sum_i n_i Z_i^2 / n_e \quad . \tag{3}$$

From formulas (2) and (3) one can obtain Z_{eff} from the following equation:

$$Z_{eff} = \frac{\varepsilon_\lambda T_e^{1/2} \lambda^2}{1.89 \times 10^{-28} n_e^2 \bar{g}_{ff} \exp[-12400 / T_e \lambda]} . \tag{4}$$

The value of $\bar{g}_{ff}$ is given by Karzas and Latter [10]. This value has a T_e dependence. However, the dependence is weak in the range of electron temperatures observed in ATF, CHS and W7-AS. $\bar{g}_{ff}$ is approximated with the following equation in the range $0.1keV \leq T_e \leq 2keV$:

$$\bar{g}_{ff} = 1.35 T_e^{0.15} \tag{5}$$

The final result is that Z_{eff} has a dependence of $T_e^{0.35}$.

Thus, we can calculate the Z_{eff} value as a function of n_e and T_e. In some cases, however, it is difficult to get a reliable time trace for T_e for every shot in a series of discharges, although the time trace of n_e can usually be obtained as a line-integrated value. Therefore, we use T_e calculated from the diamagnetic energy (T_e-W_p) as input data for determining Z_{eff}.

When the stored plasma energy W_p (kJ) and the line-averaged electron density $\bar{n}_e$ (cm^{-3}) are measured, the electron temperature T_e (eV) is given by

$$T_e = \frac{10^3 W_p}{1.6 \times 10^{-19} \bar{n}_e V} \left(\frac{W_e}{W_p} \right), \tag{7}$$

where V (cm^{-3}) is the total plasma volume of W7-AS. It is equal to $3.95 \times 10^3 a_p^2 cm^{-3}$ (R=200cm). A parabolic profile shape is assumed. The average plasma radius is mainly a function of the rotational transform and becomes smaller for an increasing edge rotational

transform. The average plasma radius is also, to a smaller extent, a function of the plasma pressure, and higher β values lead to a smaller plasma radius. This effect becomes larger for increasing edge rotational transform. The minor radius takes values from 14 cm to 17.5 cm in standard operation. W_e (kJ) is the stored electron energy and the ratio W_e/W_p gives the fraction of electron kinetic energy to the total stored plasma energy. The ratio W_e/W_p can be calculated from the results of T_e (Thomson scattering) and T_i (active NPEA) measurements [11] as a function of the electron density by the following relation :

$$W_e/W_p=C_o+C_1*N+C_2*N^2+C_3*N^3+C_4*N^4+C_5*N^5, \qquad (8)$$

where

$$N=\bar{n}_e/n_o. \qquad (9)$$

Here, n_o (cm^{-3}) stands for a critical density at which T_e is close to T_i, and $\bar{n}_e$ is the line-averaged density in units of cm^{-3}. For ECH plasmas n_o takes values of $3x10^{13}cm^{-3}$ and $6x10^{13}cm^{-3}$ in the cases of 70GHz and 140GHz, respectively. For NBI plasmas the ratio of W_e/W_p is taken to be constant and is equal to 0.62, which means that $T_e=T_i$. It is assumed that Z_{eff} is 3. The coefficients are given by

$$\begin{aligned} C_o &= 0.90065715624 \\ C_1 &= -0.32093206273 \\ C_2 &= 1.6476755707 \\ C_3 &= -3.4872729662 \\ C_4 &= 2.5422717521 \\ C_5 &= -0.60591553153. \end{aligned} \qquad (10)$$

The ratio of W_e/W_p obtained in this way is shown in Fig.4.

The value of T_e determined by this method is subject to some uncertainty. This uncertainty is estimated to be roughly 20%. However, the value of Z_{eff} is not very sensitive to variation of T_e. The dependence of Z_{eff} on T_e is shown in Fig.5. This shows that the uncertainty of 20% in determining T_e yields a revision of only 7% for the Z_{eff} value obtained in the manner mentioned above.

4. Z_{eff} MEASUREMENT AND COMPARISON BETWEEN ATF, CHS AND W7-AS

The validity of the Z_{eff} measurement in this study is examined in an ECH discharge whose electron density is scanned as a function of time. The traces of the plasma parameters for that discharge are shown in Fig.6. The electron density is raised to $4x10^{13}cm^{-3}$ during fundamental heating using two 70GHz gyrotrons, and in the next step it reaches $8x10^{13}cm^{-3}$ by changing to second harmonic heating and using a single 140GHz gyrotron.

Figure 7 shows the time behavior of the bremsstrahlung emission (5202Å) measured in the same discharge. The time behavior is exactly the same as for the electron density behavior except for the initial phase (<0.03sec) and final phase (>0.87sec) of the discharge . The bremsstrahlung emission is plotted versus the line-averaged electron density, as shown in Fig.8. If the data showed exclusively the signal arising from bremsstrahlung, it would be scaled by the solid curve like a function of n_e^2. The fitting curve is indicated by the solid line, showing the expected behavior very well.

The value of Z_{eff} can be obtained direct from the emission indicated in Fig.7. The result is shown in Fig.9(a). The determined values of Z_{eff} are relatively high in the low-density region of less than $2x10^{13}cm^{-3}$ ($t \leq 0.33$sec). There is no reason for the Z_{eff} value changing so rapidly at a time of 0.33sec. Therefore, it is reasonable to take into account that the offset value of 0.425 (10^{10}phs./s/cm^{2}str.Å) in the fitting function indicated in Fig.8 originates from line radiation emitted in a wavelength range near 5202Å. By taking this offset value into account by subtraction, the Z_{eff} value can be corrected as shown in Fig.9(b). The time trace obtained shows very reasonable behavior and finally one can obtain a Z_{eff} value of 2 in the case of ECH heating. Obtaining the Z_{eff} value in such a low-density region of less than $2x10^{13}cm^{-3}$ is an extremely successful result. Suppression of metallic impurities by boronization is probably a reason for that.

Figure 9(c) shows a time trace of the Z_{eff} value calculated by means of T_e (T_e-SX) measured from a bremsstrahlung continuum in the soft X-ray region. When we compare the data of Figs.9 (b) and (c), the Z_{eff} value obtained from the T_e-SX shows an enhancement of 12%. This means that the electron temperature calculated with equation (7) is smaller than that measured. However, the difference is very small. Furthermore, the difference is expected to become much smaller in the case of NBI, because the central T_e is close to the calculated T_e-W_p. Therefore, the use of T_e-W_p does not lead to severe deviations of Z_{eff} in this study.

The results of the Z_{eff} measurements are summarized in Fig.10 for NBI discharges in W7-AS and compared with results from ATF [7] and CHS. The discharges are selected for operation at B_t near 1T and for co-injection NBI. The NBI input power is smaller in the case of W7-AS than for the other machines. However, the Z_{eff} values do not change even in the case of higher NBI power. In the case of counter-injected NBI, higher Z_{eff} values of 3 to 6 are frequently observed. Nevertheless, good discharges with low Z_{eff} values are obtained in some cases, especially in high-density operation in combination with co-injected NBI. Discharges in CHS show the same tendency. The comparison is not made for counter-injection NBI.

The result indicates a clear difference in the wall conditioning. Especially in the range of n_e less than $5\times10^{13}cm^{-3}$ the Z_{eff} values are much smaller in W7-AS than in ATF and CHS. Of course, it is clear that the large Z_{eff} values in ATF and CHS originate in the concentration of the titanium impurity. It is amazing that even with a small input power of 0.4MW good discharges are obtained for NBI plasmas in W7-AS. NBI discharges in CHS are never realized with such a small input power. This fact clearly indicates the validity of the boronization.

The attainable densities are also high enough in W7-AS NBI discharges and reach up to $1.3\times10^{14}cm^{-3}$ in 1.25T operation. In ATF and CHS, however, they stay below $1\times10^{14}cm^{-3}$ in 1T operation (typically $8\times10^{13}cm^{-3}$). It has to be studied in the future whether the reason originates in the difference between the stellarator and heliotron/torsatron or not. Of course, there are differences in the

wall treatment, plasma-wall distance and fast ion orbit. In CHS the Z_{eff} value becomes small in the low-density region when the plasma-wall distance is increased by a prolate configuration. However, the density limit does not change.

5. ANALYSIS OF REHEAT-MODE DISCHARGES

A typical reheat-mode discharge with ECH is shown in Fig.6, as mentioned above. An increase in the stored energy is observed at a time of 0.46sec directly after switching off the gas puff during the 70GHz ECH phase. This effect also appears in the 140GHz ECH phase at a time of 0.83sec. The cut-off density for the 140GHz heating is estimated to be more than $1.2 \times 10^{14} cm^{-3}$, and it depends on the launched mode and the position of the resonant field [12]. The electron density profile is not so steep and especially in the high-density region it becomes flat [1]. The saturation which appears in the stored energy after 0.78sec does not originate in the cut-off range of the ECH pulse.

Since the deposition power of the ECH does not depend on the gas puff rate as a matter of course, the energy confinement time is really improved after the gas puff is switched off. The stored energy obtained during the course of the experiment is plotted as a function of the line-averaged electron density, as shown in Fig.11. The data are summarized only for the 70GHz ECH phase. The behavior of the stored energy during the gas puff phase conforms very well to the LHD scaling [13], denoted by a solid line. In the high-density range, however, the data deviate from the scaling, in both the 70GHz and 140GHz cases. The stored energy reaches up to 7.1kJ after the gas puff is switched off. The reheat-mode discharge affords an improvement of roughly 20% for the discharge with gas puff in this case and 10% for the given scaling level.

The Hα intensity in the reheat-mode discharge is compared with the gas puff case shown in Fig.12. The Hα signal (Hα_11) is obtained from the horizontal diagnostic port (M3-5') at a toroidal angle of 120 deg. away from the section at which the gas puff is carried out (see Fig.2). Therefore, the signal does not contain any Hα

emission direct from the gas puff section and from the vacuum wall. The quantity $H\alpha/\bar{n}_e$ indicates the edge neutral density. The figure shows that the neutral density decreases as a result of the increasing density. Especially, for the reheat-mode the density of the edge neutrals becomes lower than for the case with gas puff. The reduction of the Hα emission is observed in every Hα detector installed on W7-AS. It is clear that the particle confinement time τ_p is improved, although the absolute value of τ_p is not obtained because of the difficulty of summing the Hα intensity over the whole plasma surface.

Figure 13 shows the Z_{eff} values obtained from the same discharges as in Fig.12. Z_{eff} increases from 1.7 to 2.7 during the reheat-mode discharge. From this result we suppose that the confinement time of the impurities increases and peaking of the pressure profile occurs. The scattering of the Z_{eff} data in the low-density region ($<2\times10^{13}cm^{-3}$) originates from the raw signal and/or PMT detector fluctuations as seen in Fig.9(b). If the data are smoothed, the scattering disappears. Therefore, it is appropriate to take into account that the Z_{eff} is constant even for varying electron densities. There is a tendency for the Z_{eff} value not to depend so strongly on the electron density, at least in ECH discharges with 70GHz fundamental heating.

A reheat-mode discharge in NBI plasma (B_t=1.25T) is shown in Fig.14. The neutral beam is injected with a port-through power of 0.45MW from 0.2sec to 0.5sec. The gas puff rate is gradually reduced from 0.38sec and is completely turned off at 0.43sec. The Hα emission (M3-5'), which has a negative polarity, begins to decrease at 0.41sec and the stored energy starts to increase from 0.415sec. The stored energy reaches up to 5.8kJ in this case. This higher stored energy is maintained for 0.05sec until the end of the NBI pulse. The electron density is also kept on a constant level of $4.8\times10^{13}cm^{-3}$ during the same period.

The relation between the stored energy and the electron density is plotted in Fig.15. The data from the NBI discharges with and without gas puff are indicated by solid circles. These data show the same tendency as the LHD scaling versus the electron density.

However, the stored energy (open circles) in the reheat-mode discharge shows a considerably higher value. The discharge gives an improvement of roughly 50%. Generally, it is estimated that the deposition power of NBI increases when the gas puff is completely turned off. Of course, the deposition power of NBI is enhanced especially in the plasma center. However, the greater part of the increase in the W_p originates in the plasma outer region. In addition, it is observed that in the phase of the reheat-mode the electron temperature does not change at the plasma center. So, the improvement should be produced at the plasma outer region.

In Fig.15 the values of the stored energy are smaller than the LHD scaling. However, the absolute value of the stored energy frequently depends on the conditions of the vacuum wall and the neutral beam injector. Therefore, the main purpose is not to compare the relation between the stored energy and the LHD scaling. However, it can be seen that the properties of the reheat-mode discharge does not change even in the case where the stored energy is close to the LHD scaling.

The $H\alpha/\bar{n}_e$ value is plotted versus the electron density in Fig.16. The reduction of the neutral density is saturated in the high-density region ($5 \times 10^{13} cm^{-3}$). When the gas puff is turned off, this provokes a high-density discharge with very low-density hydrogen neutrals.

The Z_{eff} values are also obtained from the same experimental sequence. This is shown in Fig.17. The result indicates the increment of Z_{eff} from 1.7 to 2.8, whereas the Z_{eff} values do not depend on the electron density in the gas puff case. This feature is the same as in the case of ECH. In this analysis of Z_{eff} the offset is not subtracted from the signal. The soft X-ray signal at the central chord also shows a large increase in the same discharge.

Figure 18 shows the relation between τ_E and τ_p, obtained from the same sequence. Here, it is taken into account that the value of the stored energy divided by the port-through power is equal to τ_E, and τ_p is taken in arbitrary units from the local $H\alpha$ measurement (M3-5'). From the figure it is clear that the improvement of τ_p brings an improvement of τ_E. This relation is completely the same

for both the gas puff and reheat-mode discharges. Of course, in this scenario it is assumed that the limiter and wall Hα emissions do not play an important role. At least it can be understood that the reduction of the typical Hα emission (such as M3-5') from the plasma itself introduces the improvement of τ_E.

6. SUMMARY

The effective charge (Z_{eff}) of the W7-AS stellarator is measured with visible bremsstrahlung as a chord-integrated value. The measurement is carried out with an instrument brought from NIFS. The data are analyzed by the same method as used in CHS. From the measurement in W7-AS it is found that the reliability of the bremsstrahlung signal obtained is very high and that the metallic impurities are well suppressed by the boronization. As a result, the Z_{eff} value is successfully obtained even in the case of low-density ECH plasmas ($\leq 2 \times 10^{13} cm^{-3}$). Typical values of Z_{eff} observed in W7-AS range from 1 to 2 for NBI plasmas and from 1 to 3 for ECH plasmas.

The results are compared with the ATF and CHS heliotron/torsatron in the case of NBI plasmas. A reduction of Z_{eff} is observed for the W7-AS plasmas in relation to the other machines. Especially, this effect is dominant in the low-density region lower than $4 \times 10^{13} cm^{-3}$. It is clear that the reason is to be sought in the different wall conditioning, either boronization or titanium gettering.

The Z_{eff} analysis is also applied for reheat-mode discharges which are observed for both ECH and NBI in W7-AS. The increase in Z_{eff} is observed with an increase in the stored energy for both of them. It is found that the improvement of τ_p occurring after the gas puff is switched off leads to an improvement of τ_E and this feature is the same as for the CHS heliotron/torsatron.

ACKNOWLEDGMENT

This work was carried out as an IPP-NIFS collaboration financially supported by the Japanese Ministry of Education. The

authors wish to thank all members of the W7-AS group for their cooperation in conducting this research and for valuable discussions. In particular, one of the authors (SM) is grateful to H.Ringler, G.Kühner, A.Weller, D.Zimmerman, J.Saffert, W.Zeppelin and H.Yamada for their kind help and to F.Wagner for his support. The authors are also grateful for the encouragement given by K.Pinkau (Director of IPP), Y.Hamada, M.Fujiwara and A.Iiyoshi (Director of NIFS).

REFERENCES

[1] K.S.Dyabilin, U.Gasparino, H.Maaßberg et al., in Proceedings of the 19th European Conference, (Innsbruck, 1992) EPS, Petit-Lancy, Switzerland **16C** (1992) I-493.

[2] H.Iguchi, K.Ida, S.Morita et al., in Proceedings of the 19th European Conference, (Innsbruck, 1992) EPS, Petit-Lancy, Switzerland **16C** (1992) I-517.

[3] G.Herre, P.Grigull, F.Sardei, J.Kisslinger and W7-AS team, in Proceeding of 9th International Workshop on Stellarators (Garching, 1993) IAEA, Vienna (1993) 375.

[4] R.Brackel, W7-AS team and ECRH group, in Proceedings of 9th International Workshop on Stellarators (Garching, 1993) IAEA, Vienna (1993) 369.

[5] S.Morita, H.Yamada, T.Ozaki et al., in Proceedings of 9th International Workshop on Stellarators (Garching, 1993) IAEA, Vienna (1993) 542.

[6] K.Kadota, M.Otsuka, J.Fujita, Nucl. Fusion **20** (1980) 209.

[7] S.Morita, R.K.Richards, L.D.Horton, R.C.Isler, E.C.Crume and M.Murakami, ORNL-Report (1991) TM-11737.

[8] S.Morita, H.Yamada, H.Iguchi, et al., in Plasma Physics and Controlled Nuclear Fusion Research 1990 (Proc. 14th Int. Conf. Würzburg, 1992) IAEA-CN-56/C-2-5 (1993).

[9] W.Finkelnburg, T.Peters, Handbuch der Physik **28** (1957) 79.

[10] W.J.Karzas, R.Latter, Astrophys. J. Suppl. **55** (1961) 167.

[11] R.Jaenicke, W7-AS team and NI group, in Proceedings of 9th International Workshop on Stellarators (Garching, 1993) IAEA, Vienna (1993) 18.

[12] V.Erckmann, W7-AS team, NBI team et al., in Proceedings of 9th International Workshop on Stellarators (Garching, 1993) IAEA, Vienna (1993) 18.

[13] S.Sudo, et al., Nucl. Fusion **30** (1990) 11.

FIGURE CAPTIONS

Fig.1 Transmission curve of interference filter used for measurement of visible bremsstrahlung.

Fig.2 Toroidal location of Hα and visible bremsstrahlung detector in W7-AS.

Fig.3 Cross-sectional view of port M3-5' (ϕ=-10.2°). The viewing angle of the detectors is indicated by a hatched area.

Fig.4 Ratio of the stored electron energy W_e to the total stored plasma energy Wp as a function of line-averaged electron density $\bar{n}_e$ normalized to a critical density n_o. The solid circles denote results calculated from the measurement and the solid line indicates a fitting curve of the data.

Fig.5 Calculation of the electron temperature dependence of the Z_{eff} value.

Fig.6 ECH discharge (B_t=2.5T) of W7-AS used for examining the Z_{eff} measurement. The discharge also shows the ECH reheat-mode operation.

Fig.7 Raw signal of visible bremsstrahlung near 5202Å obtained from the discharge shown in Fig.6.

Fig.8 Relation between visible bremsstrahlung intensity and line-averaged electron density. The solid circles are experimentally obtained data and the solid curve is a best fitting curve as a function of $\bar{n}_e^2$.

Fig.9 Comparison of the Z_{eff} values obtained from the ECH discharge shown in Fig.6. (a) direct Z_{eff} calculation from raw signal without background offset subtraction. (b) Z_{eff} calculation with background offset subtraction. (c) Z_{eff}

calculation using electron temperature derived from a soft X-ray continuum.

Fig10 Comparison of the Z_{eff} values measured in the ATF and CHS heliotron/torsatron and W7-AS stellarator. The data are taken from similar discharges of NBI plasmas

Fig.11 Stored plasma energy of ECH plasmas (B_t=2.5T, 70GHz) as a function of line-averaged electron density. The solid circles indicate the gas puff discharge, and open circles the reheat-mode discharge. The solid line denotes LHD scaling.

Fig.12 Hα intensity divided by the electron density as a function of line-averaged electron density in ECH plasmas (B_t=2.5T, 70GHz) measured from the optical fiber set at the M3-5' port.

Fig.13 Z_{eff} values as a function of line-averaged electron density in ECH plasmas (B_t=2.5T, 70GHz). The scattering of the data in the density region of $1\text{-}2\times10^{13}\,cm^{-3}$ originates in the signal and/or photomultiplier fluctuations. No smoothing is done.

Fig.14 NBI discharge of W7-AS (B_t=1.25T) with reheat-mode operation. The Hα signal has negative polarity.

Fig.15 Stored plasma energy as a function of line-averaged electron density. The data from the discharges without gas puff are limited to a narrow density region. The difference in the stored energy between the gas puff and reheat-mode discharges is indicated. The LHD scaling denoted by the solid line is only an indication of the comparison. Comparison of the LHD scaling and the data from W7-AS is not the main purpose.

Fig.16 Hα intensity divided by the electron density as a function of line-averaged electron density in NBI plasmas (B_t=1.25T) measured from the optical fiber set at the M3-5' port.

Fig.17 Z_{eff} values as a function of line-averaged electron density in NBI plasmas (B_t=1.25T).

Fig.18 Relation between τ_E (W_p/P_{NBI}) and local τ_p ($\overline{n}_e/H\alpha$) in arbitrary units obtained from the M3-5' Hα signal. The data show a fairly good linear relation.

Transmission rate of interference filter

5202Å for visible Bremsstrahlung ($\Delta\lambda$=30Å)

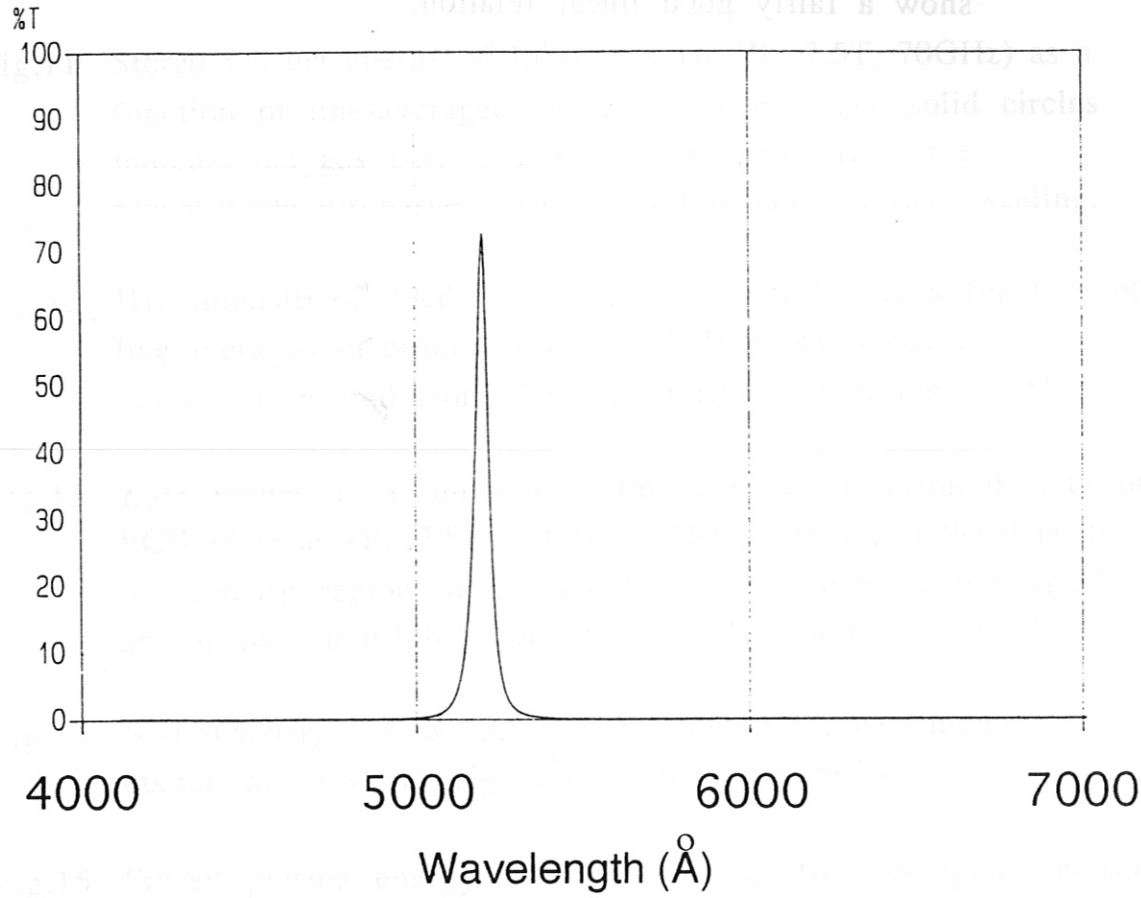

W7-AS toroidal location of the detectors

Port: M3-5'

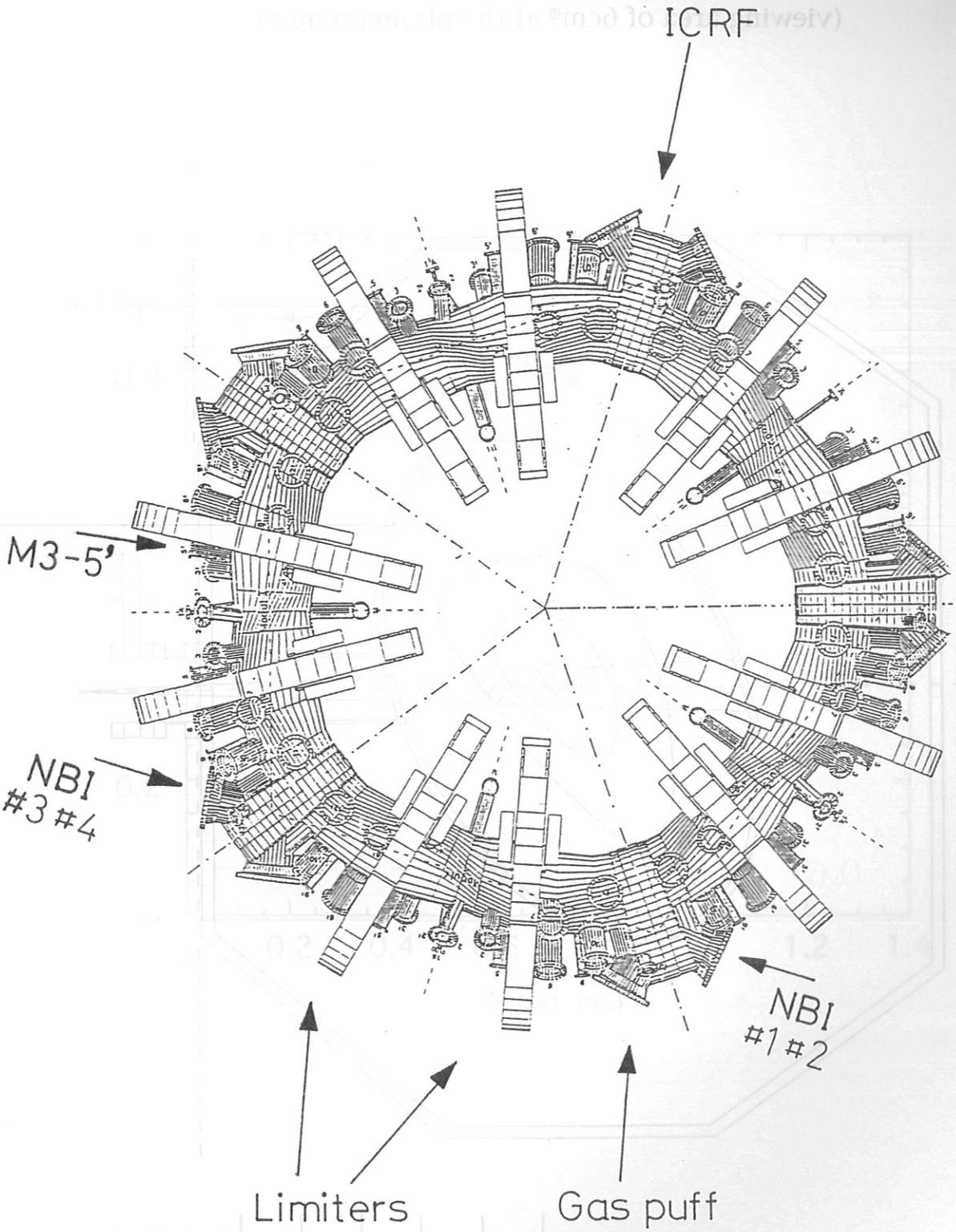

Fig. 2 S. Morita

W7-AS poloidal location of the detectors

Port: M3-5'

(viewing area of 6cmϕ at the plasma center)

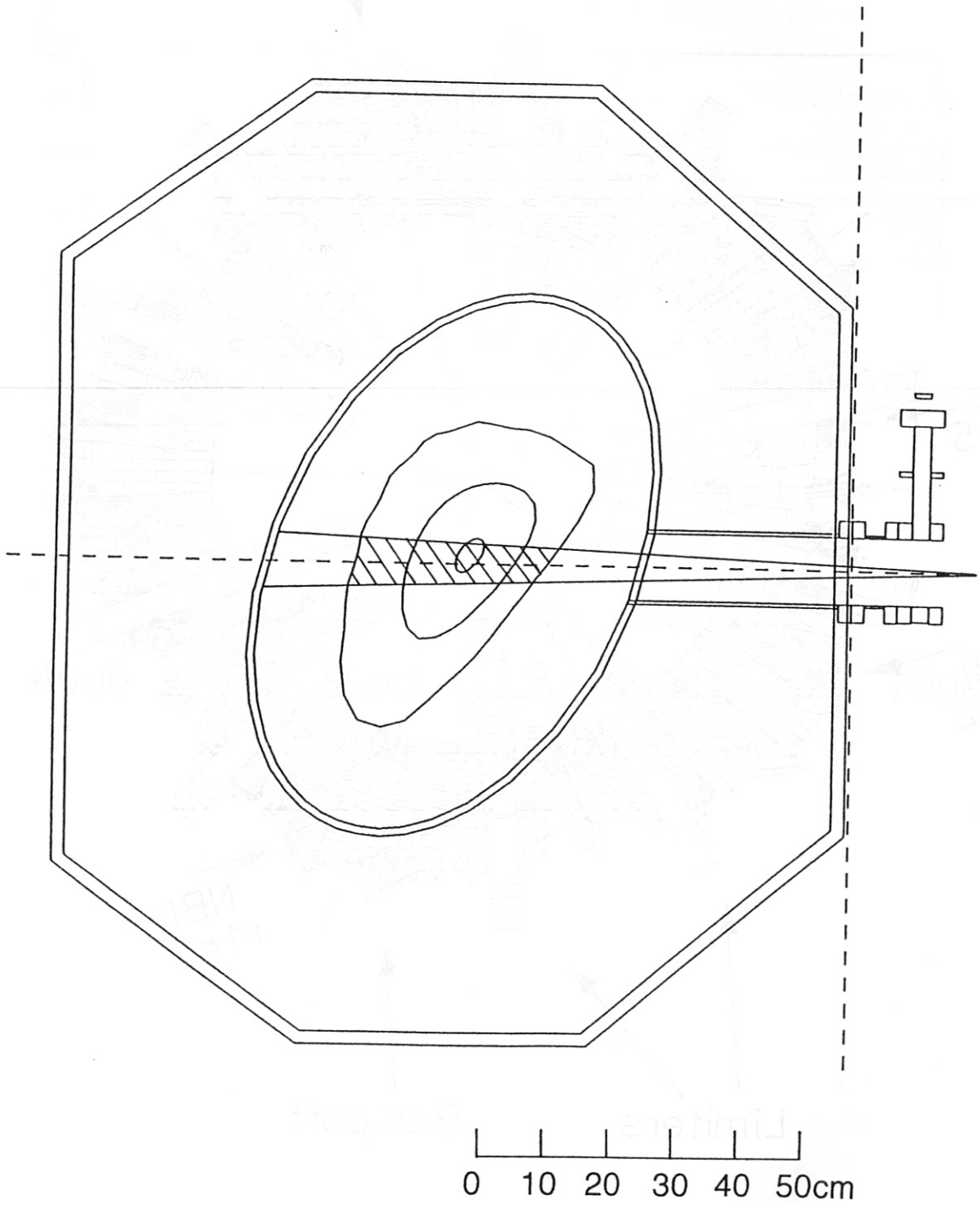

Fig. 3 S. Morita

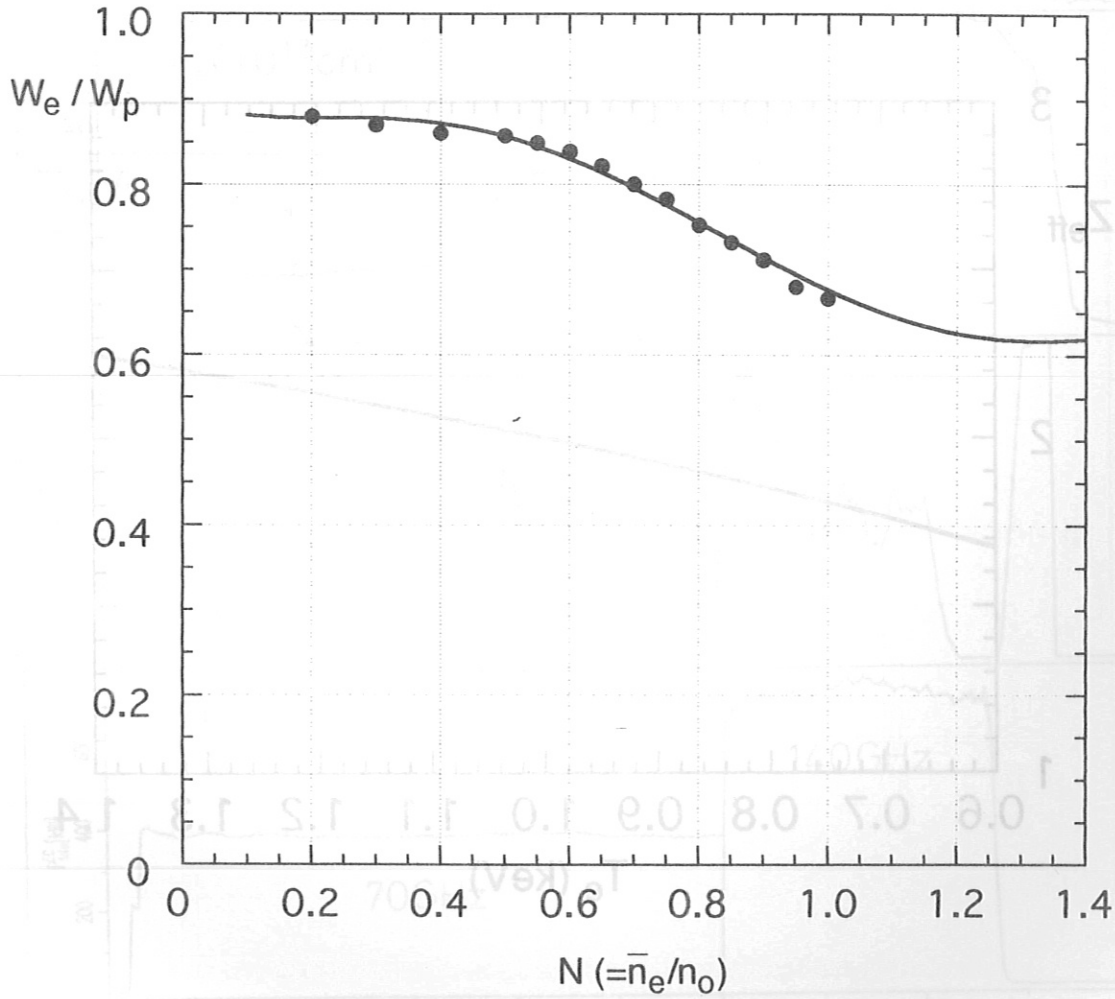

Fig. 4 S. Morita

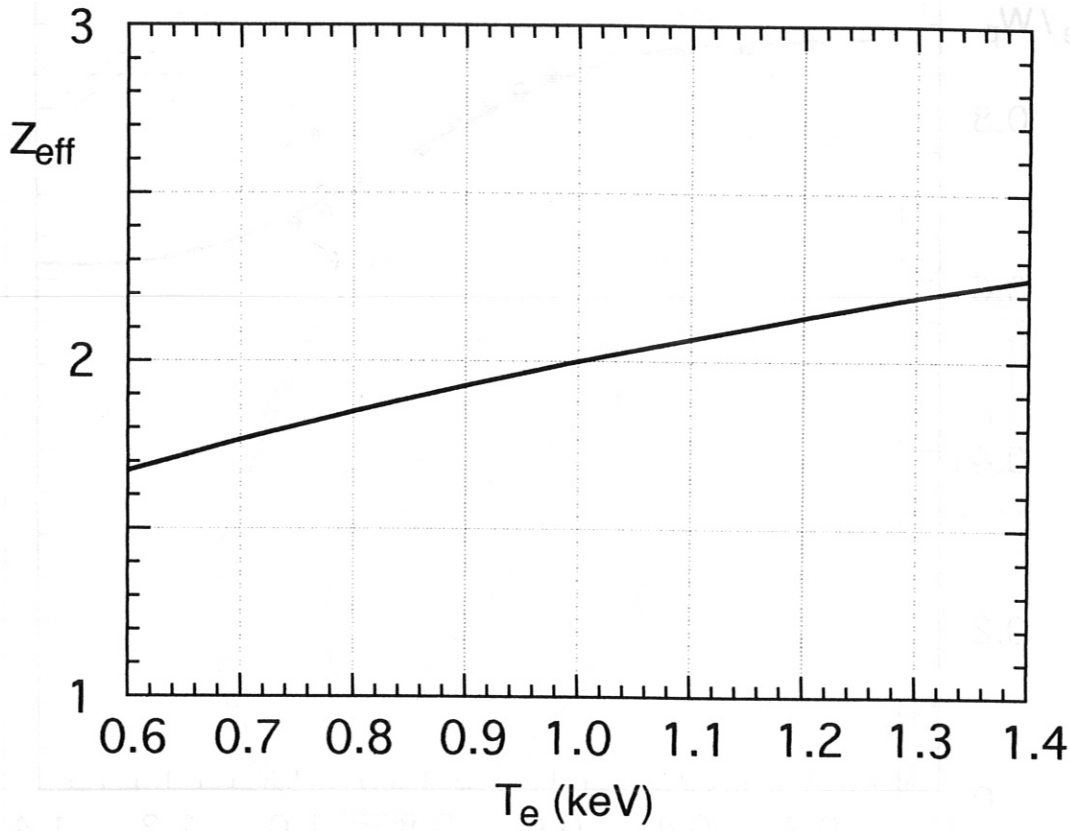

Fig. 5

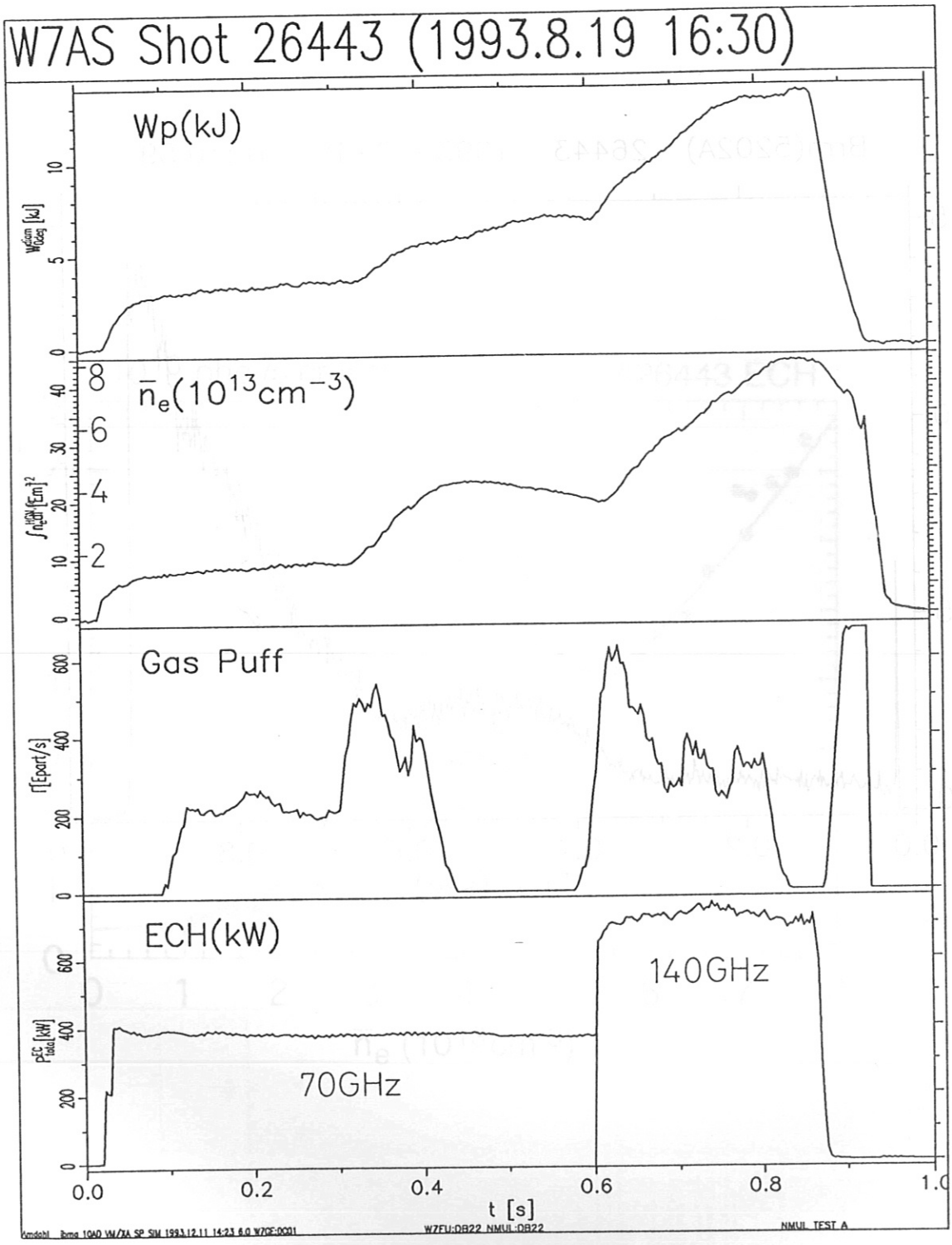

Fig. 6 S. Morita

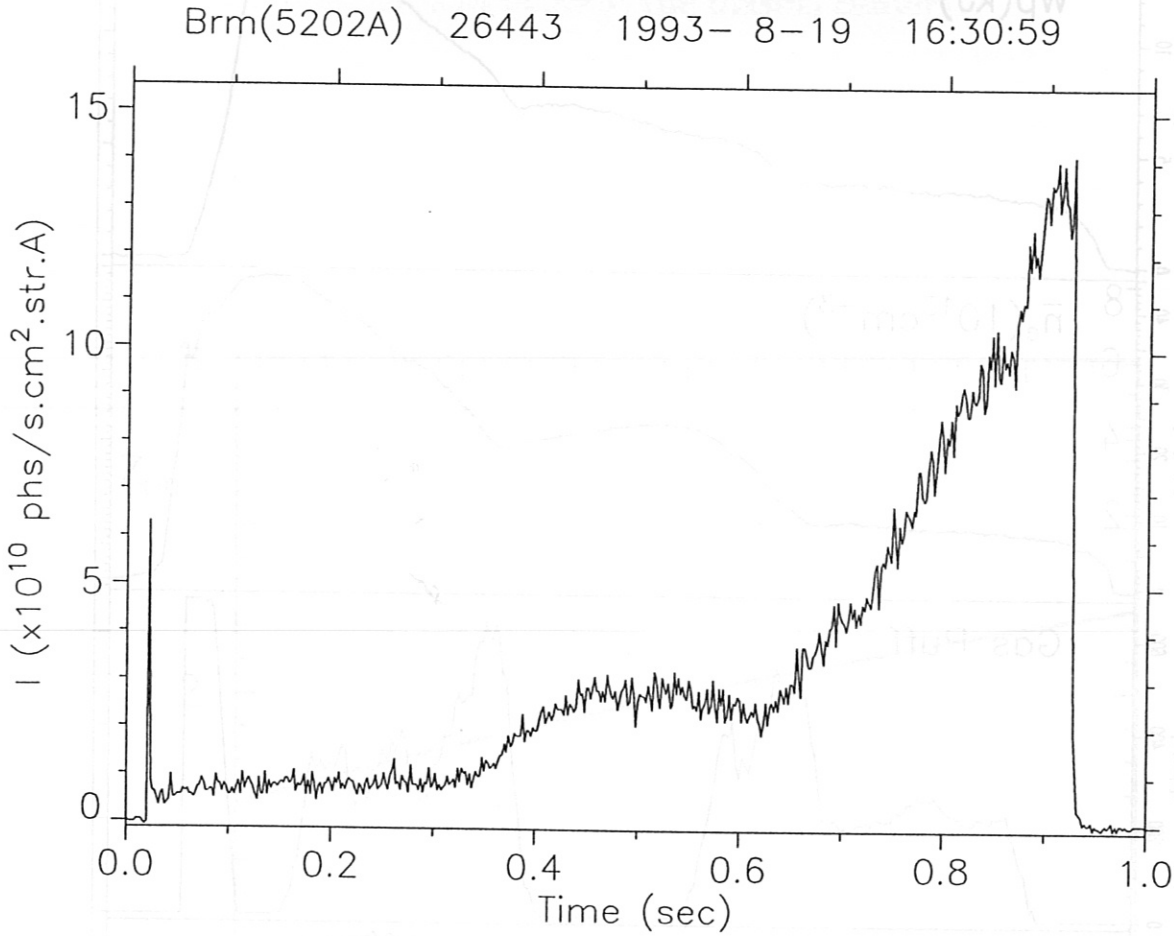
Brm(5202A) 26443 1993– 8–19 16:30:59
I (x10^10 phs/s.cm^2.str.A)
15
10
5
0
0.0
0.2
0.4
0.6
0.8
1.0
Time (sec)

Fig. 1 S Mania

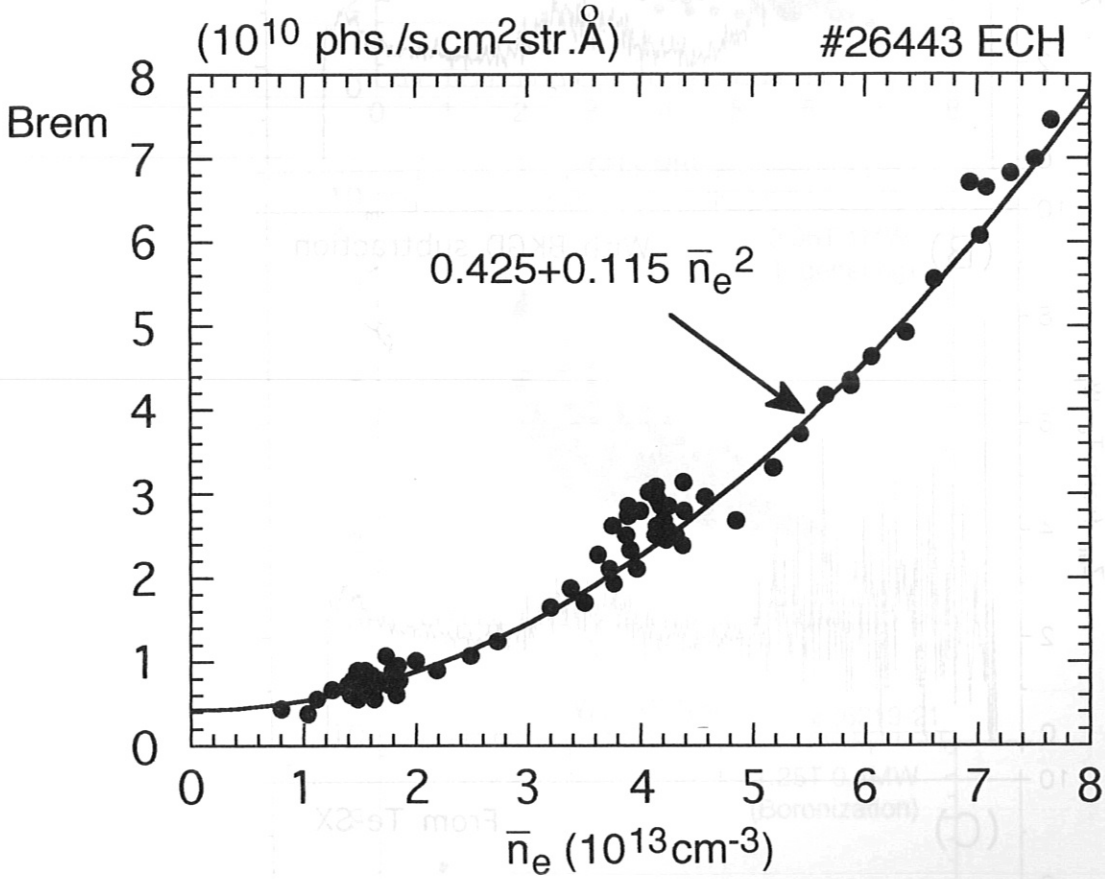

Fig. 8 S. Morita

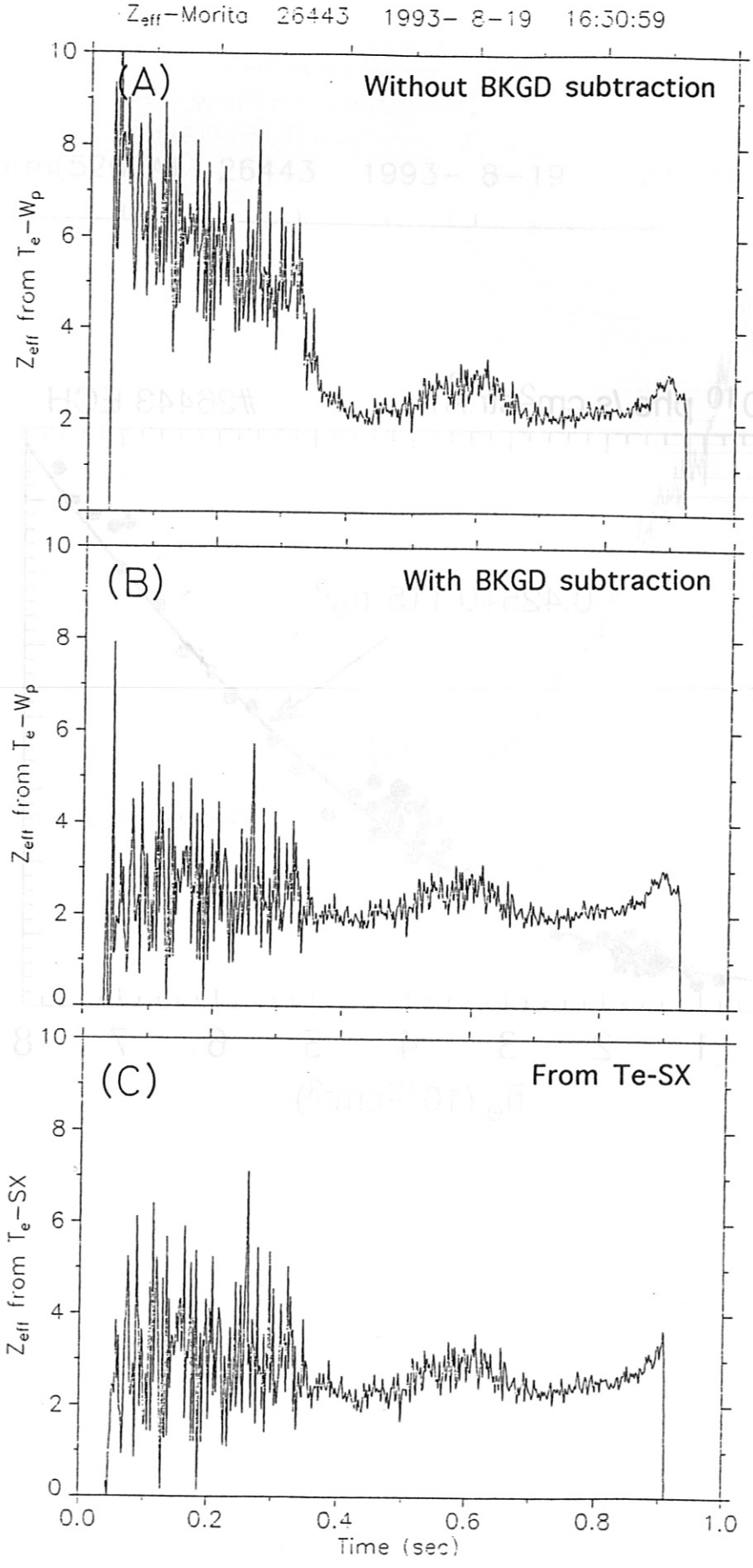

Fig. 9 S. Morita

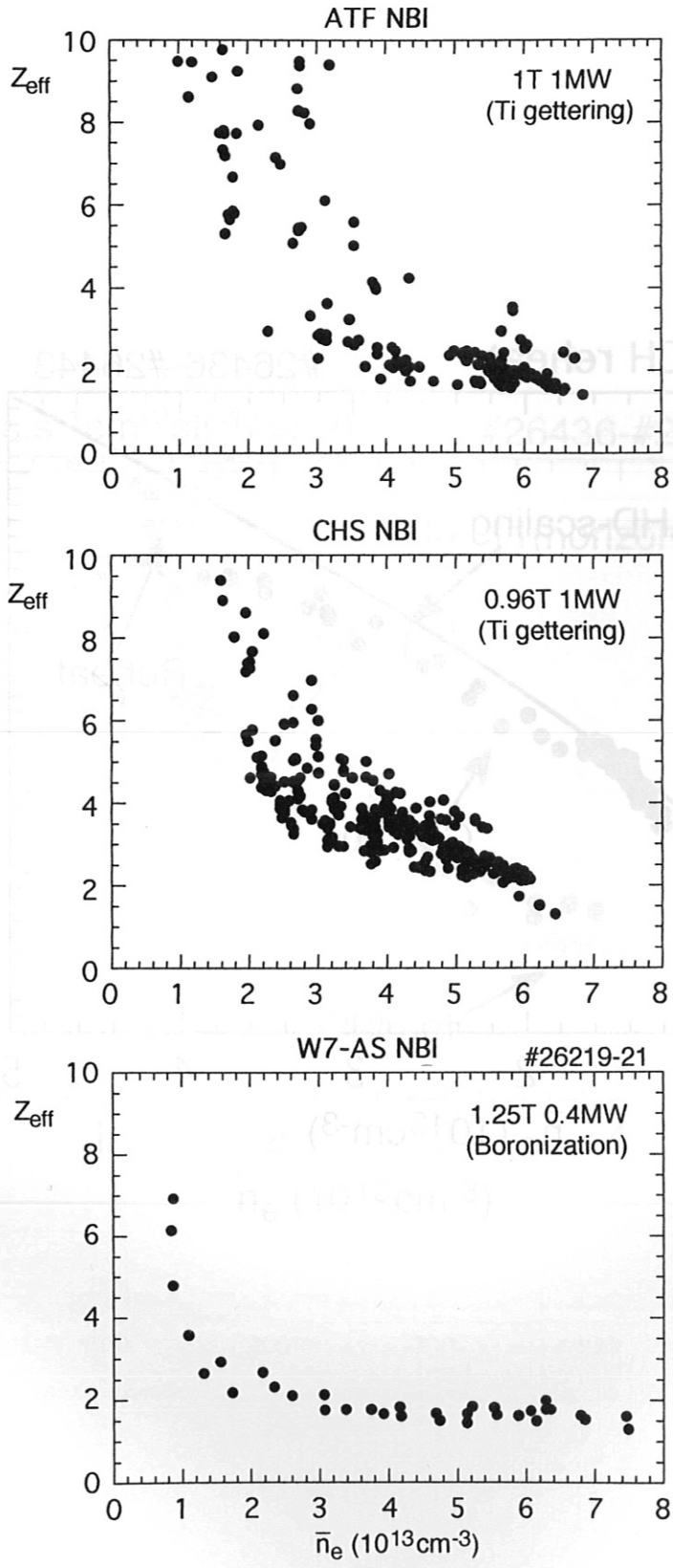

Fig. 10 S. Morita

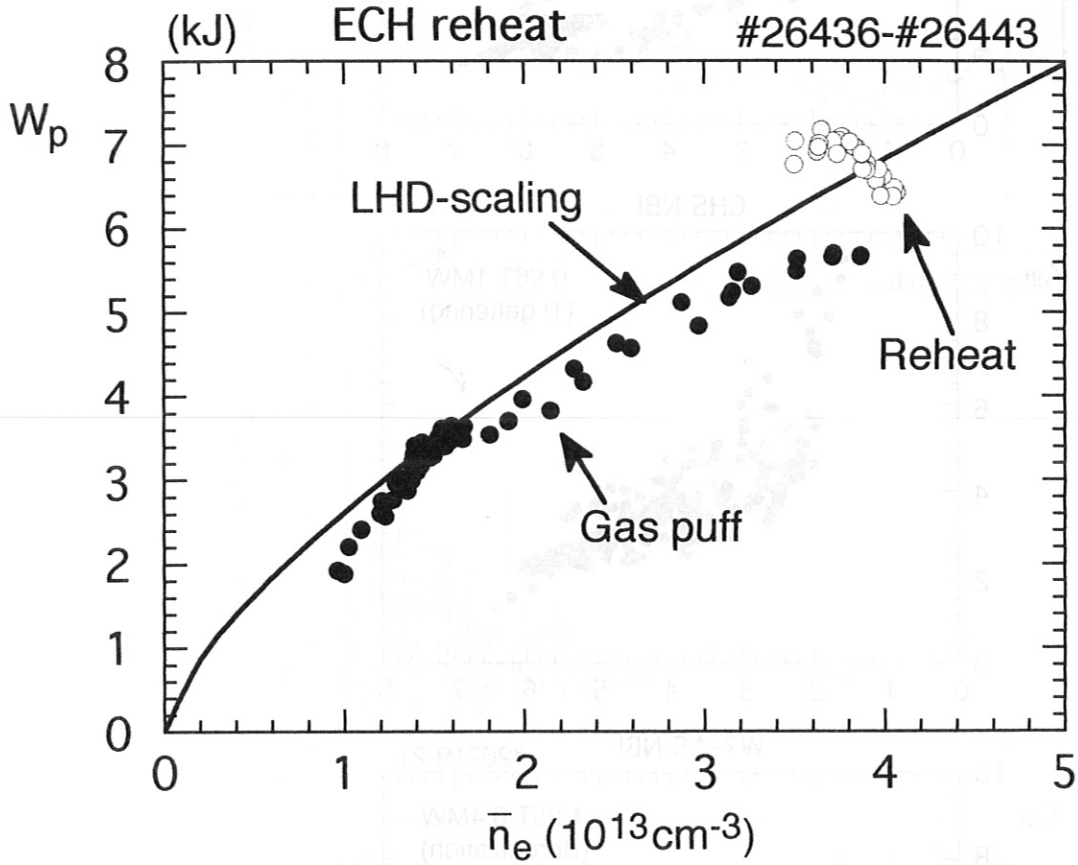

Fig. 11 S. Morita

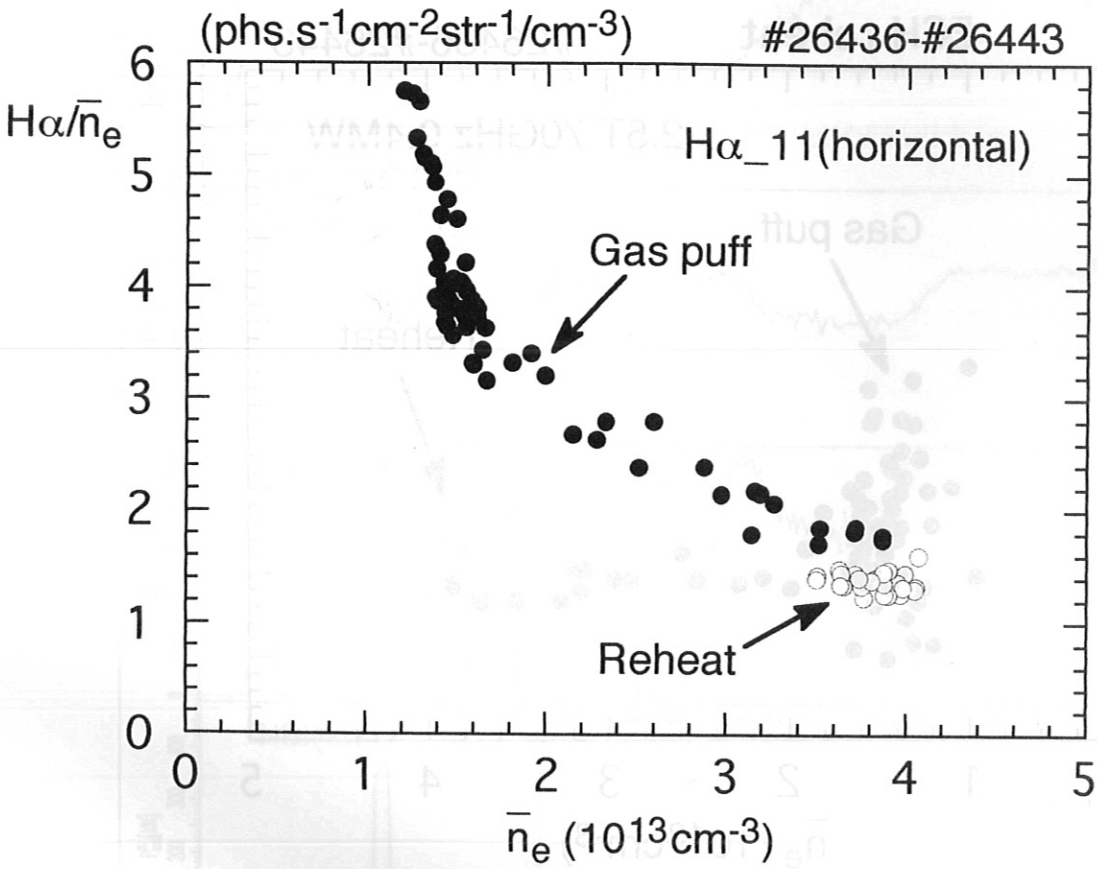

Fig. 12 S. Morita

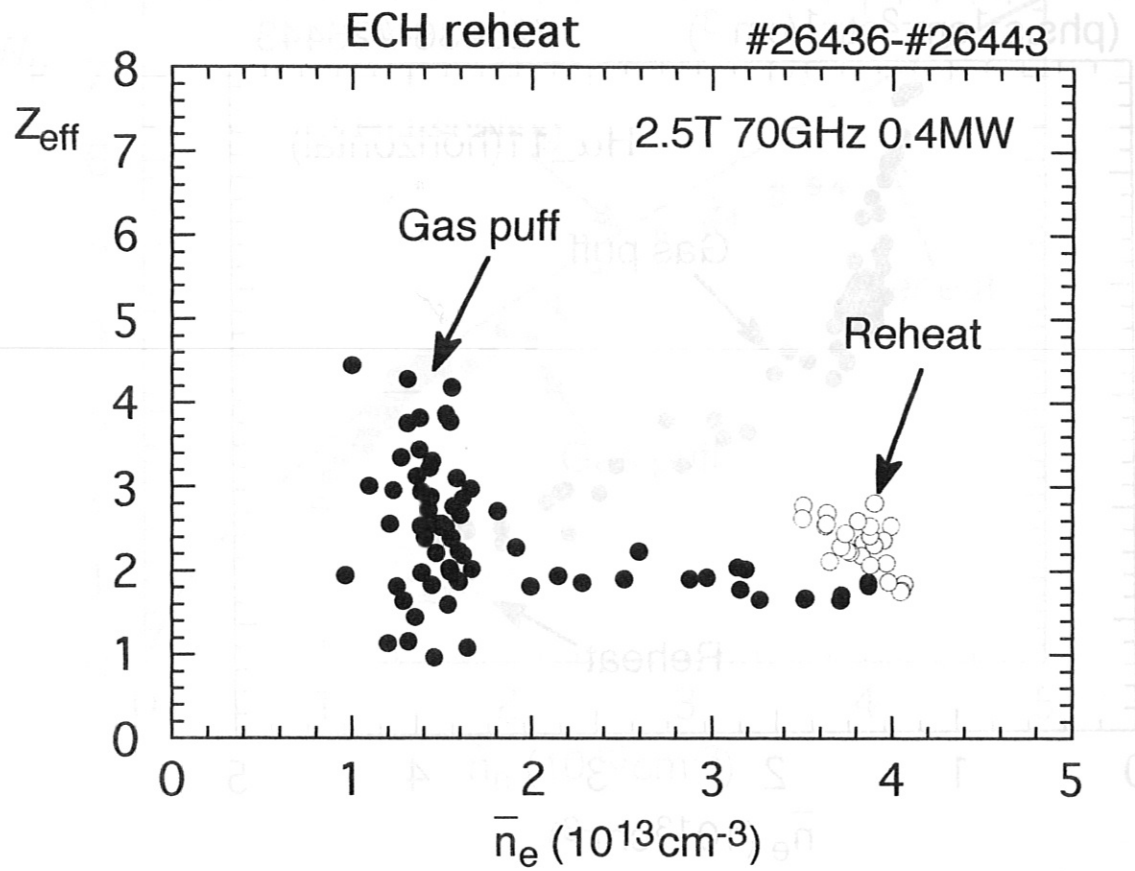

Fig. 13 S. Morita

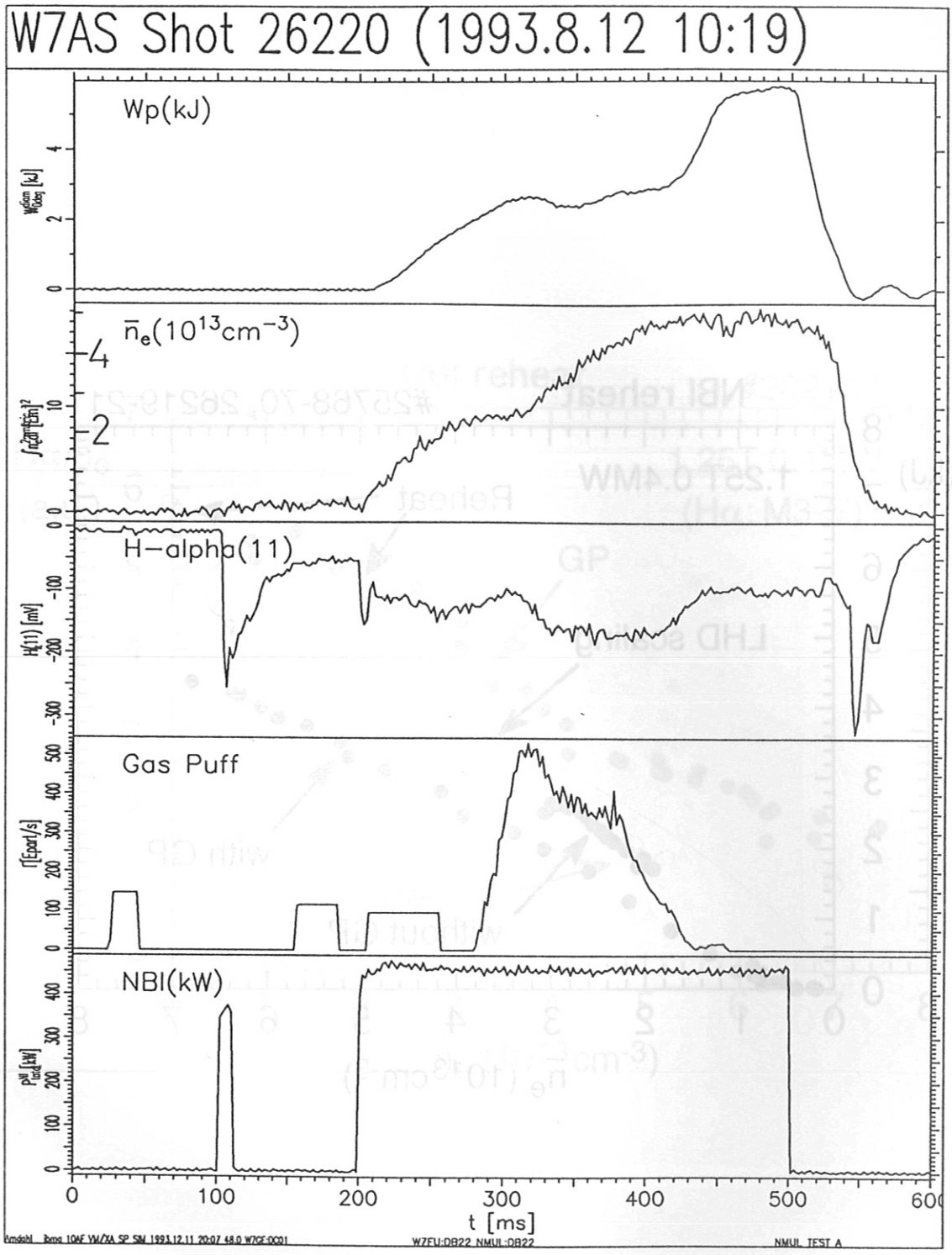

Fig. 14

S. Morita

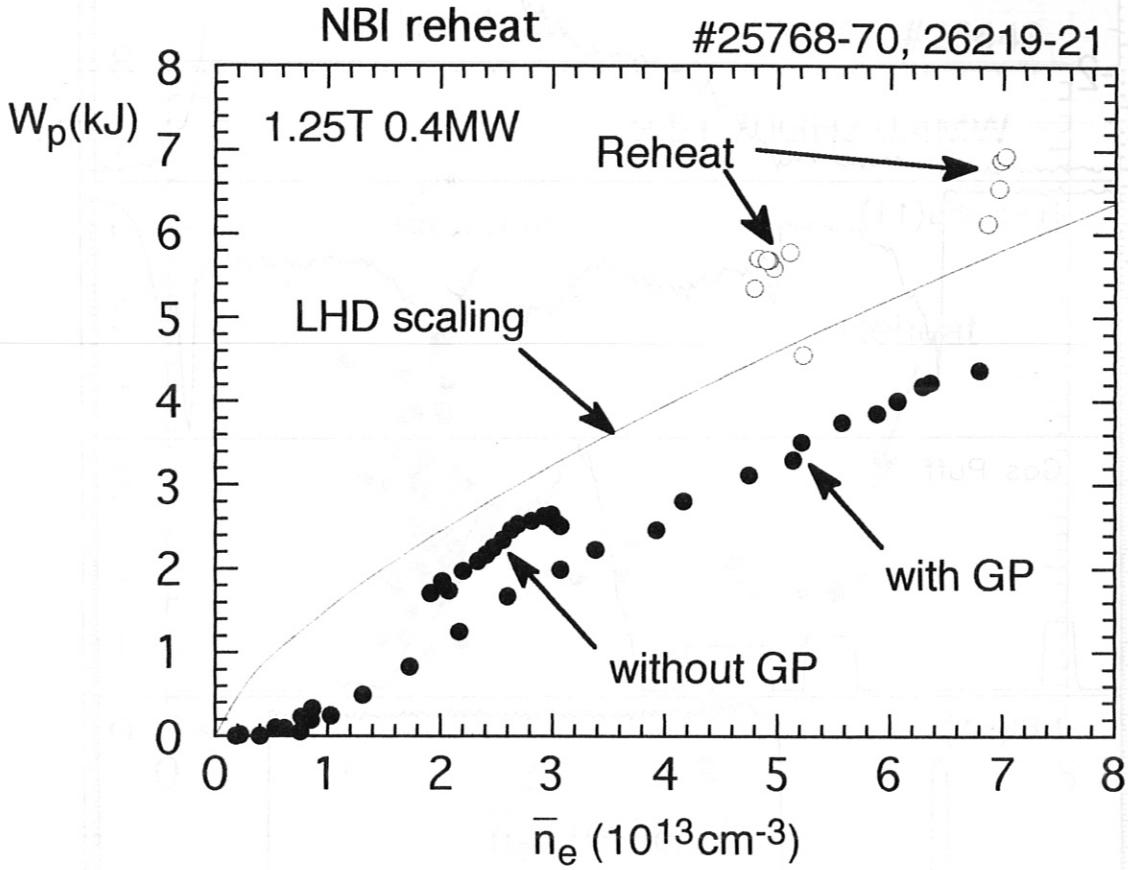

Fig. 15 S. Morita

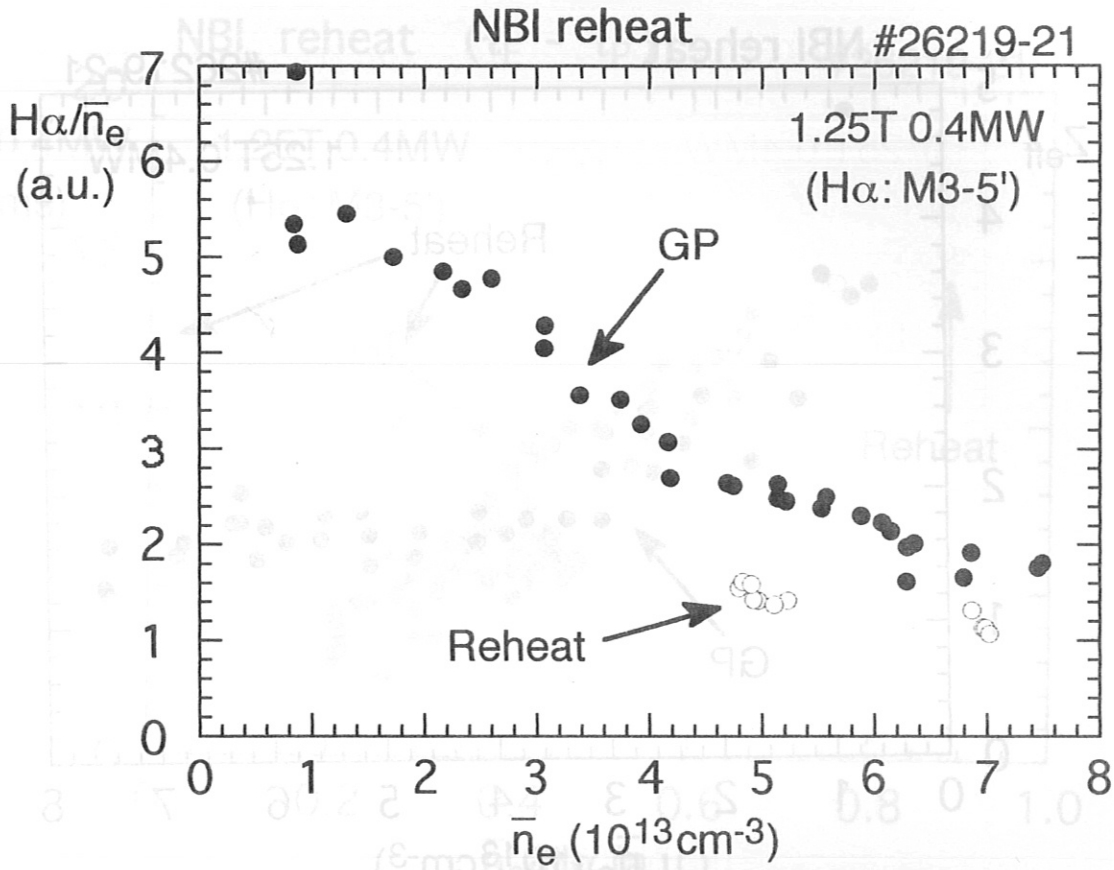

Fig. 16 S. Morita

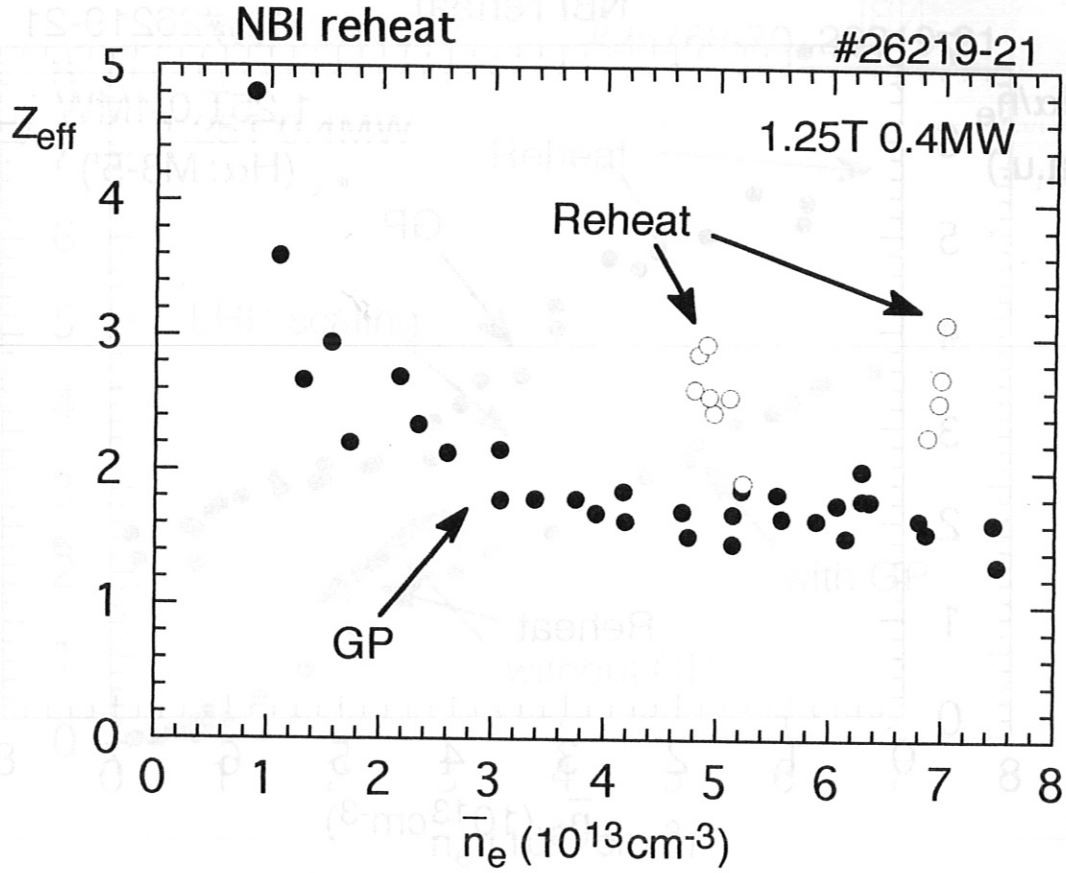

Fig. 17 S. Morita

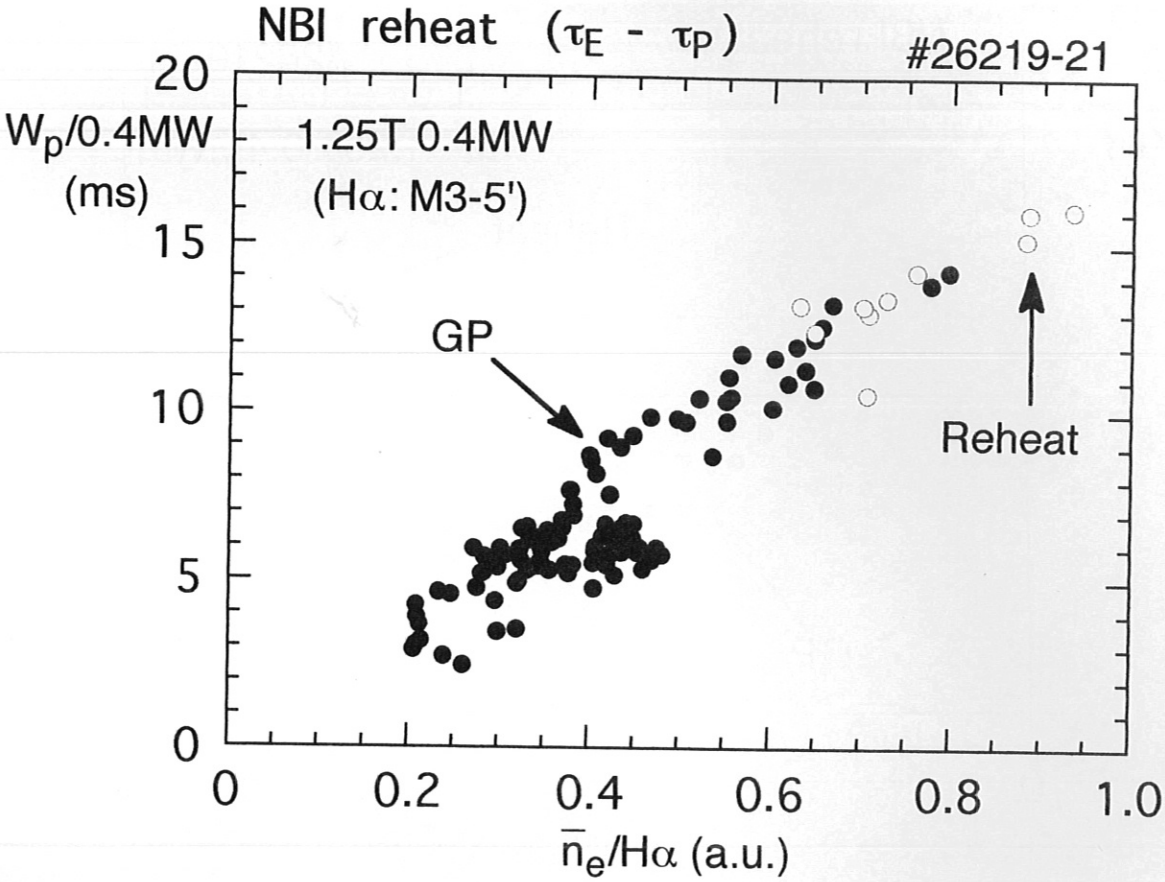

Fig. 18 S. Morita